Available online at www.sciencedirect.com
ScienceDirect
Trans. Nonferrous Met. Soc. China 31(2021) 595−608
Transactions of Nonferrous Metals Society of China
www.tnmsc.cn

Flow behavior and fracture of Al−Mg−Si alloy at cryogenic temperatures

Danielle Cristina Camilo MAGALHÃES, Andrea Madeira KLIAUGA, Vitor Luiz SORDI

Department of Materials Engineering, Federal University of São Carlos−UFSCar,
Rod. Washington Luiz, km 235, 13565-905, São Carlos–SP, Brazil

Received 28 April 2020; accepted 23 October 2020

Abstract: The tensile and fracture behaviors of AA6061 alloy were investigated in order to provide quantitative data about this alloy at cryogenic temperatures. Specimens of AA6061 alloy were solution heat treated before tensile tests at 298, 173 and 77 K and tested at strain rates in the range from 0.1 to 0.0001 s^{-1}. The results indicate the suppression of the Portevin−Le Chatelier (PLC) effect and dynamic strain aging (DSA) at 77 K. In contrast, at 298 K, a remarkable serrated flow, characteristic of the PLC effect, is observed. Furthermore, the tensile behavior at 77 K, compared with that observed at 173 and 298 K, shows a simultaneous increase in strength, uniform elongation, modulus of toughness, strain-hardening exponent and strain rate sensitivity, which is related to a decrease in the dynamic recovery rate at low temperature. These responses are reflected on the fracture morphology, since the dimple size decreases at 77 K, while the area covered by dimples increases. Comparisons of the Johnson−Cook model show that a good agreement can be obtained for tests at 173 and 77 K, in which DSA is suppressed.

Key words: cryogenic temperature; aluminum alloy; flow behavior; strain rate sensitivity; work-hardening behavior; Johnson−Cook model; fracture

1 Introduction

Stainless steel and copper alloys have been selected for several cryogenic applications for many years, such as storage and transportation in liquid cryogenics, space, biological and medical applications. In recent years, these alloys have been replaced by different alternative materials under cryogenic conditions, such as aluminum alloys, mainly due to a balance between low-density and high strength [1−3]. Nowadays, some Al alloys have also been used for building ships, liquid natural gas carriers, icebreakers and offshore plants that operated at low temperatures in polar and subsea regions [4]. Therefore, to understand the complex relations between microstructure and the mechanical response of the aluminum alloys at very low temperatures is an important effort to further develop new alloys for cryogenic uses.

The relationships between microstructure and mechanical properties of aluminum alloys have been widely investigated by experiments involving changes in temperature (room temperature and/or above) and strain rate [5−8]. However, there are only a few investigations on the effect of cryogenic temperature processing on the mechanical behavior and microstructure. For instance, a recent study by XU et al [9] performed on the AA6060-T6, showed that the fracture surfaces of tensile test specimens tested at 77 K were significantly different from those tested at room temperature. HALIM et al [10] carried out tensile tests on the AA5754 alloy at 298 and 223 K, and observed that the reduction of test temperature inhibits Portevin−Le Chatelier effect (PLC), and that solute atoms and dislocations of 223 K samples were more homogeneously distributed than those in 298 K samples. The PLC effect is observed as a serrated flow and it is related to the dynamic interaction between diffusing solute atoms and mobile dislocations, i.e. to dynamic strain aging (DSA), which can be inhibited at low

Corresponding author: Danielle Cristina Camilo MAGALHÃES; E-mail: danielle_camilo@yahoo.com.br
DOI: 10.1016/S1003-6326(21)65522-X

temperatures because the diffusion rate decreases. Two other studies on the same alloy were focused on the effect of plastic strain between 4.2 and 295 K [11] and on the texture evolution in samples with different equivalent strain degrees tested at cryogenic temperatures [12]. Finally, in the Al−Mg−Si series, ESMAEILI et al [13] examined the AA6111 alloy at cryogenic temperatures and they observed a complex behavior dependent on the nature of the obstacles to the movement of dislocations, which causes significant changes in strain rate sensitivity and work-hardening behavior.

Among Al alloys, Al−Mg−Si alloys are usually used in structural applications due to excellent mechanical strength, high corrosion resistance, good weldability and machinability [14,15]. Thus, it is important to understand the mechanical behavior of the Al−Mg−Si group particularly in terms of determining processing parameters under different conditions. Furthermore, the PLC effect at room temperature was observed to cause poor surface quality on the processed sheets, a reduction in the uniform and fracture elongations in many Al alloys [10,16,17]. Therefore, it is expected that the PLC effect could be suppressed at cryogenic temperatures, improving the final quality surface and properties of the sheets. In addition, it was concluded from the investigations of the mechanical response that both strength and ductility increase at very low temperatures [8−13,18,19]. However, far too little attention has been paid to the mechanical behavior of AA6061 alloy at cryogenic temperatures. Thereby, the experimental work presented here provides an investigation into how cryogenic temperatures affect the mechanical and fracture response of AA6061 alloy in tensile tests, in order to determine cryogenic processing parameters and to provide quantitative data about this alloy. Additionally, a constitutive equation based on the Johnson−Cook approaches was established based on the flow behavior at cryogenic temperatures of the AA6061 Al alloy.

2 Experimental

Commercial extruded bars of AA6061 alloy were received in the T6 temper condition, and the chemical composition is shown in Table 1, as obtained by optical emission spectroscopy.

Table 1 Chemical composition of AA6061 alloy (wt.%)

Si	Mg	Cu	Fe	Cr	Ti	Mn	Al
0.62	1.01	0.19	0.22	0.05	0.023	0.028	Bal.

Subsize specimens having 5 mm in diameter and 20 mm in gauge length were cut by electric discharge machining, along the extrusion direction. Uniaxial tensile tests were performed according to the ASTM E8/E8M−16ae1 Standard procedure [20]. All specimens were solution-treated at 803 K for 2 h, water cooled and immediately tested in universal testing machine Instron Model 5500R. Tests were performed at 298, 173 and 77 K, using four different initial strain rates ($\dot{\varepsilon}$) in the range from 0.1 to 0.0001 s^{-1}. Three specimens were tested for each condition (strain rate and temperature) and an average value was taken from the data. The 173 K tests were performed in a closed cryogenic chamber Instron Model 3119-610. The cryogenic chamber was cooled through a mass flow control valve connected to pressurized dewar content liquid nitrogen. The temperature was measured throughout the test making use of a type-T thermocouple positioned in contact with the specimen and the temperature error measured was ±3 K. The testing temperature was recorded using a digital data logger Fluke Model 54II. As for the 77 K tests, the specimens remained fully immersed in liquid nitrogen throughout the test. In all the low temperature tests, the specimens were kept for 10 min at that temperature before starting the test. Load and anvil displacement data were recorded throughout the tests. Engineering stress−strain curves were constructed to determine conventional tensile properties, while true stress−strain curves were used to analyze the plastic deformation behavior. The modulus of toughness in tensile tests was estimated as the whole area under engineering stress−strain curves up to the fracture point. In order to observe the fracture morphology on the fractured specimens, analyses by scanning electron microscopy (SEM) Phillips XL−30 TMP operated at 15 kV were performed. The fracture morphology was quantified by size and covered area of dimples, using 5 fields at same magnification and measuring at least 100 points in each tested condition. In addition, the area reduction (AR) was calculated using initial cross-section area measured before tests (A_0) and final cross-section area at the location of fracture (A_f): AR=$[(A_0-A_f)/A_0)]\times100\%$.

3 Results

3.1 General tensile behavior of AA6061 alloy in low temperature ranges

Figure 1(a) shows typical engineering stress−strain curves obtained at 298, 173 and 77 K, at an initial strain rate of 0.001 s^{-1}, of the AA6061 alloy in the solution-treated condition. Table 2 summarizes the engineering tensile properties obtained from Fig. 1(a). It can be seen that the tensile behavior at 77 K is quite different from the other temperatures. At 77 K, the yield stress (σ_o) increment is about 31% over the samples tested at 298 K and 20% over that tested at 173 K. For the ultimate stress (σ_u), these differences are 56% and 48% for 298 and 173 K test samples, respectively. It is worth noting that such an increase in strength is accompanied by an increase in the ductility at 77 K.

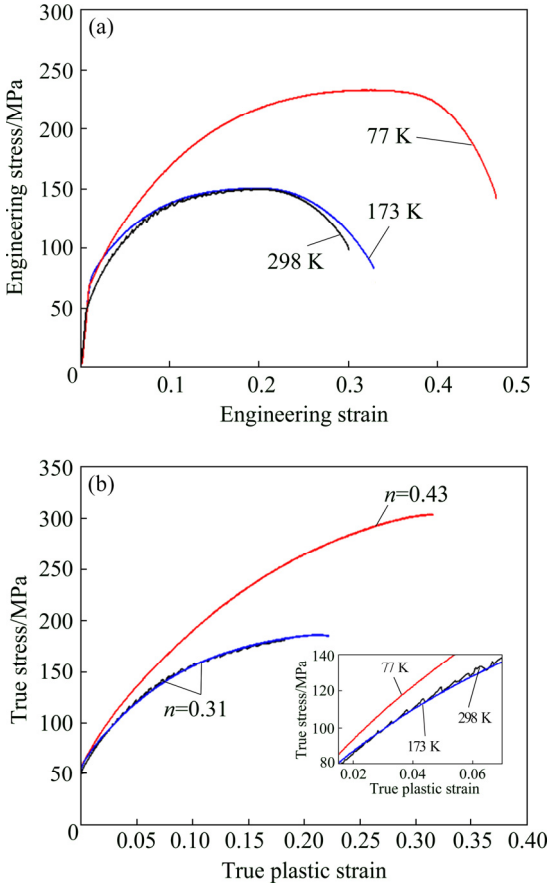

Fig. 1 Typical engineering stress−strain tensile curves (a) and typical true stress versus true plastic strain tensile curves (b) of solution-treated samples of AA6061 alloy, at 298, 173 and 77 K, with their respective strain-hardening exponent (n) (The inset shows the PLC effect; Initial strain-rate is equal to 0.001 s^{-1})

Table 2 Engineering tensile properties of AA6061 alloy in solution heat-treated condition, at different testing temperatures (Initial strain rate: 0.001 s^{-1})

Test temperature/K	σ_o/MPa	σ_u/MPa	ε_t/%	ε_u/%	AR/%
298	55±4	150±12	30±4	20±2	77±5
173	65±5	158±13	33±3	23±2	72±6
77	72±7	234±10	47±3	35±3	62±4

For instance, the total elongation (ε_t) and the uniform elongation (ε_u) at 77 K are, respectively, 56% and 75% higher than those at 298 K, as can be seen in Table 2. On the other hand, the area reduction at the location of fracture (AR) decreases at lower temperatures, a contrasting behavior which can be attributed to the strain distribution along the sample during tensile tests, in agreement with a prior investigation [9].

Figure 1(b) shows the corresponding true stress versus true plastic strain curves, where the elastic components are subtracted from the original strain data in order to consider only the plastic portion of the strain in the following analysis. The respective values of strain-hardening exponents (n) are presented and they are calculated from the linearization of the Hollomon equation ($\sigma=K\varepsilon^n$, where K is a strength coefficient and σ and ε are, respectively, the true stress and the true plastic strain). Moreover, the n value at 298 K is smaller than that at 77 K, reflecting the simultaneous increase in deformation capacity and in strain hardening observed at the lower temperature. This suggests that cryogenic deformation leads to a partial suppression of dynamic recovery, and then an increase in the dislocation density. In addition, the inset in Fig. 1(b) shows that the PLC effect decreases or disappears when the test temperature decreases.

In order to analyze the effect of different strain rates on the mechanical response of the AA6061 alloy at room and cryogenic temperatures, tensile tests were carried out with initial strain rates from 0.1 to 0.0001 s^{-1}. Figure 2 shows flow curves obtained with different initial strain rates, where a clear tendency of inversion in the strain rate sensitivity can be seen at 298 K (Fig. 2(a)), if compared to low temperature tests (Figs. 2(b, c)). Despite some experimental discrepancies, at 298 K, the yield stress and ultimate tensile stress are inversely related to the strain rate. From such a

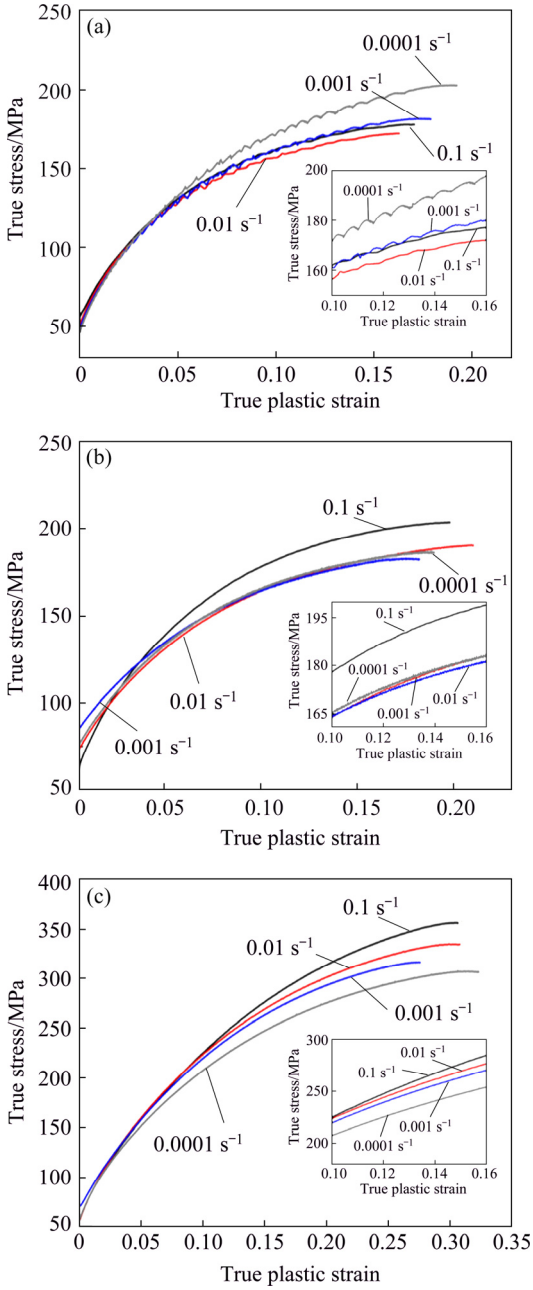

Fig. 2 Tensile test plots for different strain rates of AA6061 alloy, obtained at different temperatures: (a) 298 K; (b) 173 K; (c) 77 K

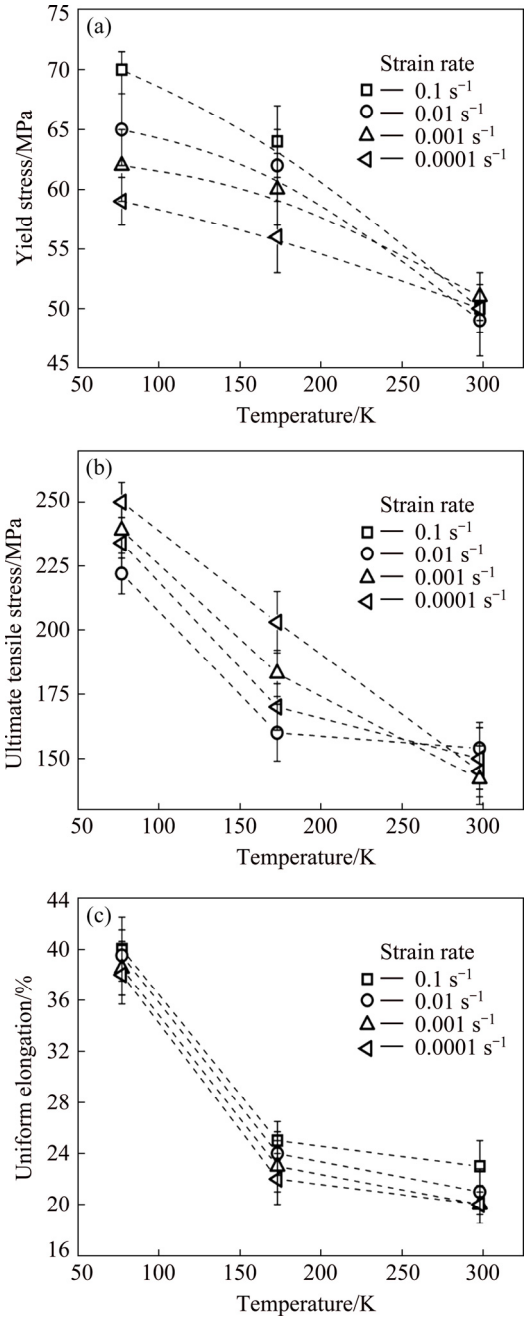

Fig. 3 Influence of temperature and initial strain rates on mechanical response of solution-treated samples of AA6061 alloy: (a) Yield stress; (b) Ultimate tensile stress; (c) Uniform elongation (Data from engineering stress−strain curves)

behavior, it would be expected that the strain rate sensitivity (m) takes negative values. Negative m can be understood as a consequence of DSA, which in turn originates the PLC effect [21−23], as observed at 298 K for AA6061 alloy in a solutionized state. Figure 3 summarizes the main parameters obtained from the engineering stress−strain curves for different strain rates and temperatures.

It can be seen from Figs. 3(a, b) that the effect of the strain rate on the strength at 298 K tends to the opposite of that observed at 77 and 173 K, as already noted for the true stress−strain plots in Fig. 2. Furthermore, regardless of the strain rate, both mechanical strength and ductility increase with decreasing temperature, and this effect is more evident at 77 K. As for elongation, Fig. 3(c) shows that it is less affected by the strain rate, but it is also sensitive to the temperature.

The strain-hardening exponent as a function of the initial strain rates and test temperatures used here are plotted in Fig. 4, as well as the strain rate sensitivity as a function of the true plastic strain.

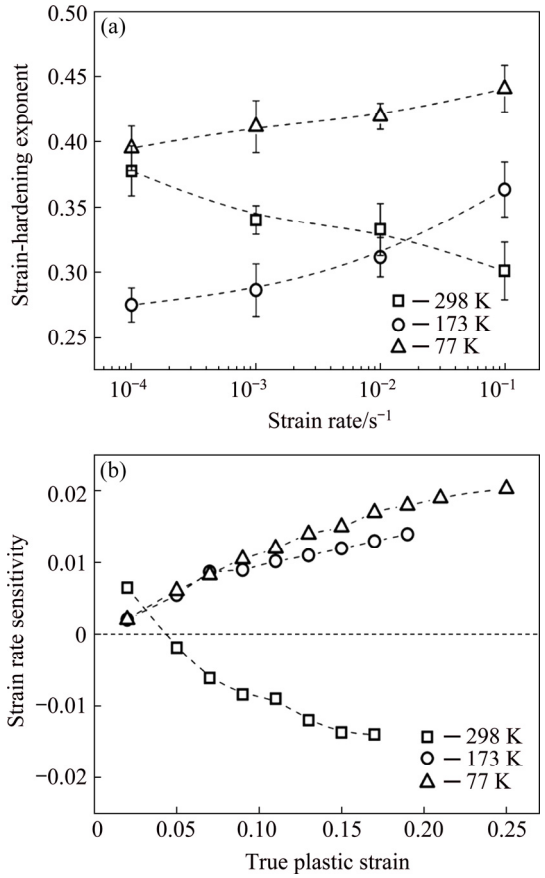

Fig. 4 Strain-hardening exponent values for different strain rates and temperatures (a), and changes of strain-rate sensitivity with true plastic strain for different temperatures (b)

From Fig. 4(a), it can be observed that, at 173 and 77 K, the AA6061 alloy exhibits an opposite trend to that observed at 298 K; n increases with the strain rate at the lower temperatures. A calculation of the average strain-rate sensitivity (m) is carried out following the usual power-law expression, which is valid at constant ε and T: $\sigma=C\dot{\varepsilon}^{m}$, where C is a hardening coefficient. Figure 4(b) shows that, at the beginning of straining, the strain-rate sensitivity is positive for all temperatures. However, after a critical true strain value, parameter m becomes negative when the plastic strain is increased at 298 K. For cryogenic tensile tests, m remains positive and increases when the plastic strain is increased at a similar rate.

The plastic deformation behavior of the AA6061 alloy tested at different temperatures and strain rates was studied in terms of the Kocks−Mecking (K−M) model. This model describes the strain strengthening as a function of the average dislocation density based on the Taylor equation, as detailed in Ref. [24]. Thus, an increase in stress induced by strain can be understood as a competition between work-hardening and dynamic recovery. Generally, when the dislocation glide is the main deformation mechanism, the K−M curves exhibit an approximately linear region known as Stage III and the slope of this region is proportional to the dynamic recovery rate, which can be described by the Voce equation [24]. Thus, the K−M model can be described by $\theta=\theta_o-K'\cdot\sigma$, where θ is the work-hardening rate ($\theta=\mathrm{d}\sigma/\mathrm{d}\varepsilon$), which comes from the true stress−true plastic strain curves; θ_o is the maximum initial work-hardening rate (estimated by the intercept with the θ-axis) and $K'=-\mathrm{d}\theta/\mathrm{d}\sigma$ represents the dynamic recovery rate, estimated by the slope of the Stage III in a plot of θ versus σ. Figure 5 shows the K−M plots in terms of the incremental flow stress ($\sigma-\sigma_o$), where σ_o is taken as the yield stress. Table 3 summarizes the main parameters from the K−M curves. For curves with serrated flow due to the DSA effect, the slope of Stage III is estimated by a linear regression over this region, as exemplified by a dashed line in Fig. 5(b).

The shape of the curves at 298 K indicates that the PLC effect is reflected in the K−M plot behavior in Stage III. Figure 5 and Table 3 confirm that θ_o, shows no significant changes with the strain rate or with the temperature and, therefore, it can be considered as a constant dependent only on the initial microstructure, as proposed by the K−M model [24]. The term $K'=-\mathrm{d}\theta/\mathrm{d}(\sigma-\sigma_o)$ is proportional to the dynamic recovery rate in Stage III. The data show that at 77 K, the dynamic recovery rate is greatly decreased compared to the other two test temperatures, i.e. the work-hardening rate decreases more rapidly in the tests performed at 298 and 173 K than those performed at 77 K, at a same incremental flow stress value.

3.2 Fractography

Aiming to gain a better understanding of the behavior of necking and fracture at low temperatures, SEM analyses were carried out. Figure 6 shows a photograph of the specimens after tensile tests in the necking region. As shown in

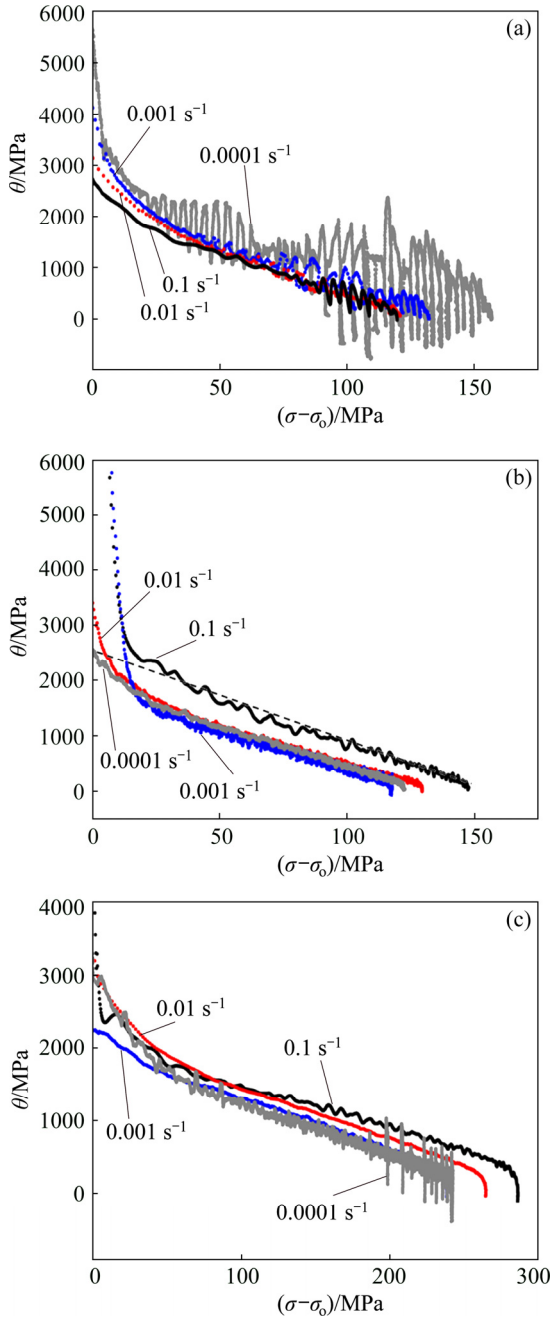

Fig. 5 K−M plots of solution-treated AA6061 alloy obtained from tensile tests with different initial strain rates at different temperatures: (a) 298 K; (b) 173 K; (c) 77 K (The dashed line in (b) represents the procedure adopted in determining the K−M parameters)

Table 2, the area reduction is smaller for the tests at 77 K, in comparison to 173 and 298 K, in contrast to that observed for total and uniform elongation, which are higher at 77 K. The predominant shape on a macroscopic analysis is the cup-and-cone fracture and the temperature exerts a strong influence on the necking, as shown in Fig. 6. PARK et al [4] found different fracture shapes at cryogenic

Table 3 Parameters of K−M plots

Temperature/K	Initial strain rate/s^{-1}	$K'=-[d\theta/d(\sigma-\sigma_o)]$	θ_o/MPa
298	0.1	16.8±1.3	2107±103
	0.01	16.6±1.5	2156±132
	0.001	15.5±1.4	2178±125
	0.0001	13.4±1.0	2272±139
173	0.1	16.5±1.6	2512±130
	0.01	13.9±1.2	1892±128
	0.001	13.5±1.1	1742±112
	0.0001	14.3±1.4	1882±131
77	0.1	5.5±0.7	2025±104
	0.01	6.9±0.8	2148±123
	0.001	6.9±0.9	2001±117
	0.0001	6.8±0.8	1913±108

tests for AA6061 alloy after T6 treatment, with flat plane surface and smaller ductility. However, they observed innumerous fine precipitates β'' in the matrix that can explain the fracture behavior at a low temperature. In the present work, the specimens are in a solutionized state, which provides relative ductility and allows necking.

The fracture surface details were analyzed by SEM and they are presented in Fig. 7. It can be observed in Figs. 7(a, c, e) that the side view is very different at low temperatures when compared to room temperature. At cryogenic temperatures, this region is much more irregular than that at 298 K, with more surface bands. Another important feature is the surface boundary of the fracture. At 77 K, this region is intensively serrated, while at 298 K the fracture boundary is smooth (also less surface bands). At 173 K, the appearance in the side view is intermediate compared to 77 and 298 K. A similar fracture morphology was found in the AA6060 alloy in a T6 treatment condition tested at 295 and 77 K [9].

In Figs. 7(b, d, f), dimples can be observed that are typical of a ductile fracture. Clearly, the test temperature has a strong influence on the dimple size and density. At 298 K (Fig. 7(b)), the fracture surface is approximately (30±1)% covered by dimples, which have an average size of (12.5±4.4) μm. For specimens tested at 173 K, it can be observed that the dimples cover (36±1)% of the fracture surface, with an average size of (6.9±3.1) μm. Finally, for specimens tested at 77 K,

Fig. 6 Photographs illustrating typical fractured specimens of AA6061 alloy after tensile tests at different temperatures showing surface bands in neck region

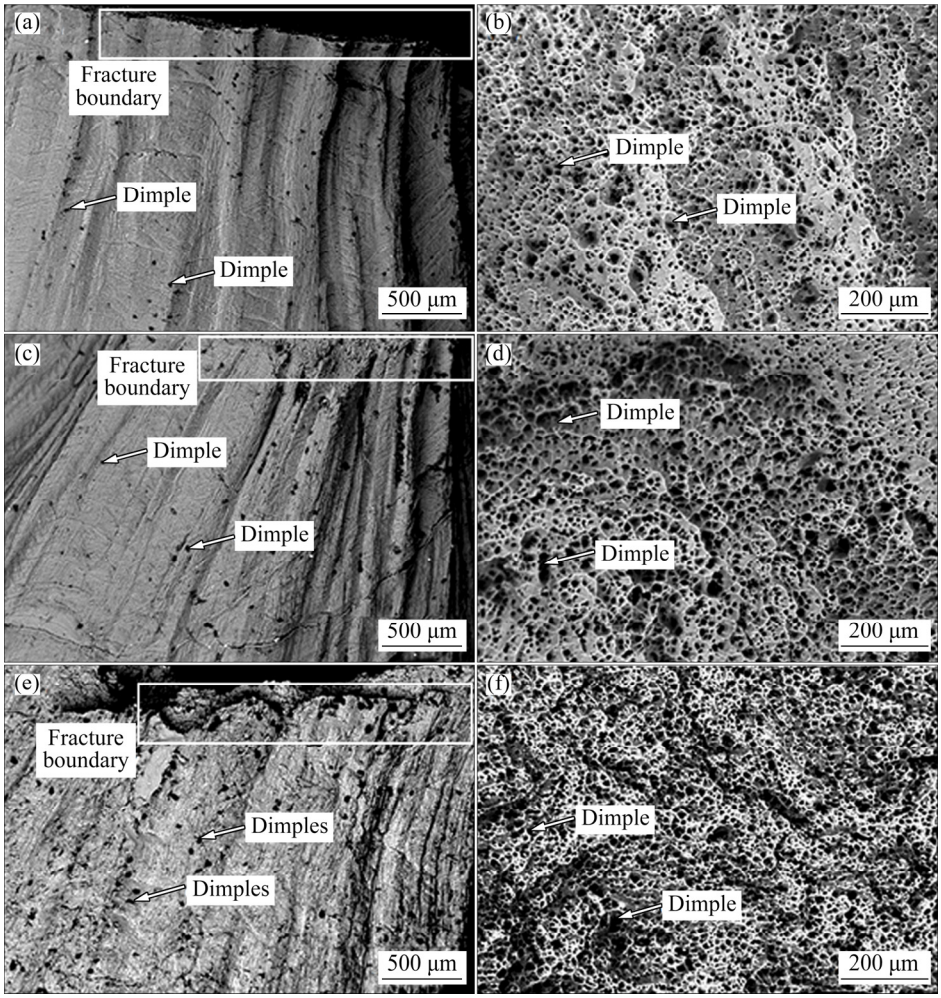

Fig. 7 SEM images for side view of fracture (a, c, e) and fracture surface (b, d, f) of AA6061 alloy after tensile test at different temperatures: (a, b) 298 K; (c, d) 173 K; (e, f) 77 K

the dimples present an average size of (5.5±2.6) μm, covering (45±2)% of the surface. Thus, the average dimple size decreases when the test temperature is reduced. Concerning the dimple's density, there is more dimples per area at 77 K than at 298 and 173 K. All these features are indicative of the amount of energy absorbed during the deformation: at the low temperature, the tensile modulus of toughness is high, and thus the morphology of dimples is affected.

Figure 8 provides a general view of the tensile behavior in terms of the modulus of toughness,

which is represented by the whole area under the stress−strain curves and gives a measure of the total work done on a unit volume of material during the test. It can be taken as the ability of the material to absorb energy in a plastic strain at different temperatures and strain rates. An interesting outcome is that at 77 K, the energy absorbed until the fracture is significantly higher than that at 173 and 298 K. In addition, it can be observed that the modulus of toughness rises when the strain rate for cryogenic tensile tests is increased, while for 298 K the trend is opposite.

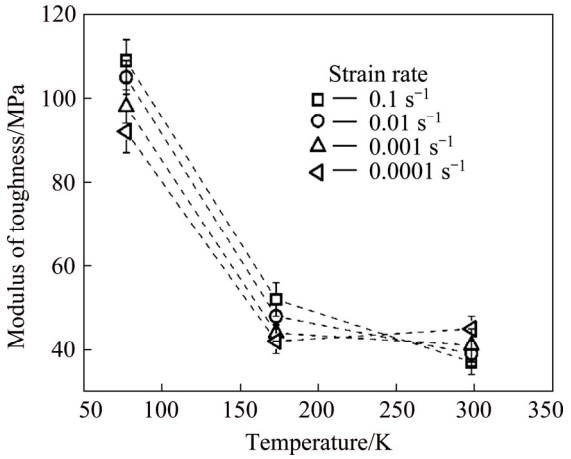

Fig. 8 Modulus of toughness as function of temperature at different tensile strain rates in AA6061 alloy

4 Discussion

The tensile behavior of the AA6061 alloy in the strain plastic domain is highly dependent on two main phenomena: dynamic recovery and DSA. Despite being competing processes, the dominant effect among the two is influenced by deformation temperature range and initial strain rate.

4.1 Effect of cryogenic temperature and strain rate on flow behavior

From the tensile tests at room and cryogenic temperatures, a total strength can be expressed as

$$\sigma=\sigma_o+\sigma_d+\sigma_{ss}+\sigma_{DSA} \quad (1)$$

where σ_o is the initial strength contribution from the pure Al matrix, σ_d is the contribution by dislocations during plastic deformation, σ_{ss} is the strength contribution from solid solution and σ_{DSA} is the dynamic strain aging contribution.

The term σ_d is strongly affected by the temperature and restoration mechanisms, such as dynamic recovery that is thermally activated. It is well-established that the thermal softening of the metallic material occurs during the deformation by two basic restoration mechanisms: dynamic recovery and dynamic recrystallization. For high stacking fault energy (SFE) alloys, such as AA6061, only dynamic recovery as a softening mechanism is expected in a wide range of temperatures and strain rates [25,26]. Dynamic recovery causes a decrease in the work-hardening rate due to the reduction in the long-range internal stresses, either by annihilation of dislocations or by forming energetically lower dislocation systems, namely substructures [25]. Thus, at 77 K, the dynamic recovery rate (K') is small and a high dislocation density is reached, which is in agreement with earlier investigations [27−30]. From the K−M data in Table 3, it can be seen that the following relationship is valid:

$$\left(\frac{d\theta}{d\sigma}\right)_{77K} \ll \left(\frac{d\theta}{d\sigma}\right)_{173K,298K} \quad (2)$$

Consequently, σ_d assumes the higher value at 77 K and lower values for 173 and 298 K. This effect may also be due to the reduction in available slip systems for dislocation motion, which occurs at low temperature; thus, promoting partial suppression of the effects of dislocation cross-slip and climb. The dynamic recovery of dislocations, which decreases the flow stress, is responsible for the positive strain-hardening exponent observed in Fig. 4. Experimental evidence for the reduction in slip systems and the reduction in dynamic recovery rate was described in Ref. [29], when the microstructural evolution in cryogenic rolling and ECAP of the same material was evaluated. Moreover, at 173 K, the strain is concentrated within microscopic shear bands, which shows evidence of a reduction in slip systems and the reduction in the dynamic recovery rate.

The second term, σ_{ss}, related to the solid solution strengthening, may be estimated by comparing pure aluminum to the AA6061 alloy, both tested at 77 K and at a low strain rate. From the literature [30], the yield stress of 99.95 wt.% Al at 77 K and an initial strain rate of 0.00019 s^{-1} is 40.1 MPa. In the present work, the yield stress of AA6061 alloy tested at the same temperature and an initial strain rate of 0.0001 s^{-1} is equal to 59 MPa. Thus, the σ_{ss} can be taken as this difference,

approximately equal to 19 MPa. It can be observed that the contribution of this term is relatively small compared to the other terms.

Finally, the last term, σ_{DSA}, can significantly contribute to the total strength, as a result of complex interactions between dislocations and solute atoms. Together with the temperature, the initial strain rate controls the speed at which various processes occur, such as dynamic recovery and DSA. Furthermore, the strain rate plays a significant role in the strain hardening process in AA6061 alloy. In the insert of Fig. 2(a), details of the intermediate region of the stress−strain curves show the change of the frequency and amplitude of stress with strain rates; when strain rate is lower, such as 0.0001 s^{-1}, DSA occurs, which is reflected in a higher strength. At higher strain rates, for example 0.1 s^{-1}, there is insufficient time for DSA to occur, and therefore the possible effect of increased mechanical strength by the solute diffusional flow acting as barriers for dislocations is not observed. Moreover, at 173 and 77 K, the effect is opposite to that observed at 298 K. The mechanical strength increases with initial strain rate, resulting in $m>0$ as DSA is inhibited at these temperatures, as shown in Fig. 4. At low temperatures, the DSA is not observed and the strain rate sensitivity becomes positive, as reported in the literature [22]. Additionally, it can be observed that yield stress and uniform elongation are significantly higher at 77 K than at 173 K.

The value of m also presents a singular behavior at 298 K compared to the cryogenic temperatures. At room temperature, m is negative, which causes increases in modulus for greater plastic strains, as indicated in Fig. 4(b). The strain corresponding to $m=0$ is called the critical strain, ε_c. In this case, at 298 K, $\varepsilon_c=0.045$ is found. According to van den BEUKEL [31], the onset of serrated flow takes place once the condition $\partial\sigma/\partial\dot{\varepsilon}=0$ is reached. In other words, the PLC effect occurs when the strain rate sensitivity becomes negative and, simultaneously, the plastic strain is higher than ε_c [22,24,31,32].

For cryogenic tests, the positive correlation of m with the true plastic strain appears to fit with the large uniform elongation observed during the tensile test, simultaneously with the smaller area reduction. This behavior is similar to that occurring in superplasticity, that is, a suppression or delay on the onset of necking. However, this effect is associated with higher values of m, and thus in this case, the justification is mainly based on the partial reduction of the mechanisms associated with dynamic recovery.

In Fig. 3(c), higher elongation values are observed at cryogenic temperatures, especially 77 K, a behavior reported for other Al alloys at cryogenic temperature [8−18]. Taking the Considère criterion [33] into account, the non-uniform deformation regime initiates after reaching the condition: $(d\sigma/d\varepsilon)=\sigma$. Thus, as shown in Table 3, the dynamic recovery rate is smaller at 77 K and the reduction of $d\sigma/d\varepsilon$ with the increase of strain is slower at this temperature than at 298 and 173 K. Therefore, the Considère criterion is reached at large strains, that is, the onset of necking is delayed at 77 K, and thus the uniform elongation is higher than that at the other two test temperatures.

Figure 4(a) shows the combined effect of the initial strain rate and temperature on the Hollomon strain-hardening exponent, which indicates the response of a metallic material to cold working. The larger the magnitude of n, the greater the work-hardening for a given amount of plastic strain. Thus, it is expected that alloys with a high strain-hardening exponent responds better to the deformation. As can be observed for 298 K tensile test, this exponent decreases when the initial strain rate increases. In contrast, for the cryogenic temperature test, the opposite trend is observed. In particular, at 77 K, the highest value of the n is measured, which increases with the initial strain rate. As the strain-hardening exponent can give a direct indication of the uniform elongation of a metal, by comparing the values of n to the uniform elongation values shown in Fig. 3(c), it can be observed that, in fact, the ductility increases at this temperature. For AA6061 alloy, the best condition for strain hardening is at cryogenic temperature, due to an increase in the strain-hardening exponent, and partial suppression of dynamic recovery and DSA.

In summary, for the 298 K tensile test, the reduction in the strain rate causes an increase in the flow stress, a response that can be attributed mainly to DSA and high dynamic recovery rate [20,22,31]. At cryogenic temperatures, however, this phenomenon is suppressed by a reduction in the solute diffusivity coefficients, together with the partial suppression of dynamic recovery, and the

consequence is the highest strength, strain-hardening exponents and ductility values at 77 K and the strain hardening is dominant over DSA strengthening.

4.2 Johnson−Cook modeling

A common approach to describe the effects of temperature and strain rate on the flow behavior is the Johnson−Cook (JC) model, which is phenomenological and considers that the strain hardening is modified independently by the temperature and the strain rate [34]. The model is presented with three terms shown by

$$\sigma=(\sigma_0+K\varepsilon^n)\left[1+C\ln\left(\dot{\varepsilon}/\dot{\varepsilon}_0\right)\right](1-T^{*m'}) \quad (3)$$

The first term is the Hollomon equation describing hardening, the second term predicts an increment of the flow stress increasing the dimensionless strain rate $\left(\dot{\varepsilon}/\dot{\varepsilon}_0\right)$, and the third is the decrease of flow stress with the increment of the relative temperature T^* (m' is a thermal softening exponent). T^* can be calculated by

$$T^*=(T-T_0)/(T_\mathrm{m}-T_0) \quad (4)$$

where T_0 is the reference temperature and T_m is the melting point (in this work, T_m=890 K [35]).

To fit this equation to the experimental data, the lowest temperature and lowest strain rate were used as references for the hardening behavior. The strain rate term was adjusted to maintain a constant temperature, and the temperature term was adjusted to maintain the strain rate constant.

The original JC model is one of the most well-known constitutive equations of dependence among temperature, strain rate and strain, due to its simple implementation and adjustment for a wide range of temperatures [34,36]. However, it is inadequate to describe some flow behaviors, especially as coupled factors of temperature and strain rate are disregarded. Moreover, strong deviations from the glide mechanism (such as twinning, Orowan strengthening, DSA, and dynamic softening) may take place. This leads to several modifications aiming to track the deformation behavior more accurately [37,38].

Using the criteria that the effect of the strain rate may be considered independently, since $\mathrm{d}(\mathrm{d}\sigma/\mathrm{d}\varepsilon)/\mathrm{d}(\sigma-\sigma_\mathrm{o})$ is a constant for the same temperature, the second term of the JC equation was calculated: $(1+0.02\ln(\dot{\varepsilon}/\dot{\varepsilon}_0))$.

To determine the exponent m', related to the temperature term in the JC flow model, the same reference strain rate data were considered, but for different test temperatures. As a consequence, the strain rate term becomes equal to 1, and then the exponent m' can be calculated. When solving Eq. (3), the value of m' is estimated equal to 0.7. Thus, the JC model for the AA6061 Al alloy is presented in Eq. (5):

$$\sigma=(530\varepsilon^{0.41})[1+0.02\ln(\dot{\varepsilon}/\dot{\varepsilon}_0)](1-T^{*0.7}) \quad (5)$$

The final fits obtained with Eq. (5) are shown in Fig. 9. From Fig. 9, it can be observed that the JC model fits better at cryogenic temperatures than at room temperature. For 77 and 173 K, the differences between the predicted and experimental data are minimal, within the dispersion range of the measurements. The JC model considers only the strain hardening effect, which is modified independently by the temperature and the strain rate, and the dynamic recovery effect is not taken into account. On the experimental curves at cryogenic temperatures, the dynamic recovery is suppressed partially, but not totally. Thus, at high strains, it is possible that some dynamic recovery competes with strain hardening, which results in a slight deviation from the JC model. Figure 1 shows that the flow behaviors obtained at 173 and 298 K are very similar, which means that the DSA phenomenon at 298 K is responsible for shifting the curve to higher stress value than that predicted by the JC model. When the DSA mechanism is activated, a clear inversion of trends is observed in terms of the strain-hardening exponent and the strain-rate sensitivity (see Fig. 4), but the JC model does not represent this behavior, as can be seen in Fig. 9(a).

The original JC model assumes that the strain hardening, thermal softening and work-hardening are independent phenomena, which may result in an inadequate prediction of the flow behavior. In a certain temperature range, the effect of the negative strain-rate sensitivity, as consequence of DSA, can be taken into account in order to modify the JC model, considering the non-linear behavior of σ concerning the strain-rate term. Thus, parameter C is modified as a function of the strain rate, $C=f(\dot{\varepsilon})$, for the tests performed at room-temperature. A function proposed by YE et al [35] to describe C for the solution-treated AA6063 Al

alloy tested at 298 K is considered in the current work, as presented in Eq. (6):

$$C=f(\dot{\varepsilon})=1.04\times10^{-9}\dot{\varepsilon}^{2}-2.63\times10^{-6}\dot{\varepsilon}^{2}+9.9\times10^{-3} \quad (6)$$

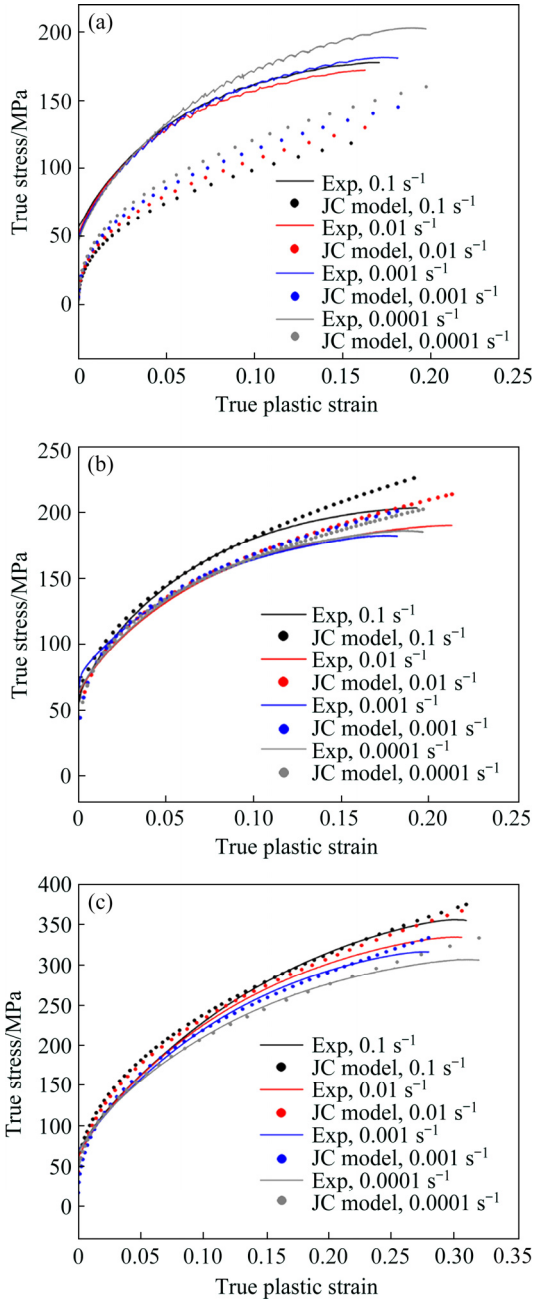

Fig. 9 Comparisons between experimental and predicted results using JC model for AA6061 alloy tested at different temperatures: (a) 298 K; (b) 173 K; (c) 77 K

Based on Eqs. (5) and (6), the new fitted curves using a modified JC model for AA6061 alloy tested at 298 K are presented in Fig. 10.

In Fig. 10, it can be seen that the fitting results from the modified JC model proposed by YE et al [35] are in good agreement with the experimental data from the tensile tests performed at 298 K. These fitting data consider the variation of the C parameter with the strain rate, according to Eq. (6). Thus, the flow behavior of the material in cryogenic temperature ranges can be fitted by the original JC model, while for room-temperature or above, the modified JC model is more appropriate.

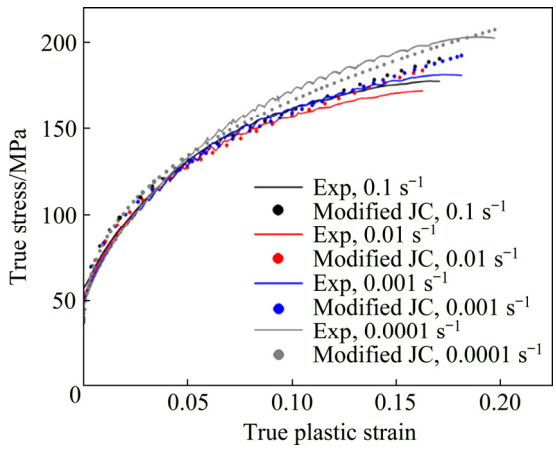

Fig. 10 Fitted curves using modified JC model for tensile data of AA6061 alloy tested at 298 K

Concerning solute diffusivity, Table 4 shows the solid interdiffusion coefficients for Mg and Si in the Al matrix, considering that the alloying elements are in a solid solution. This may explain the disappearance of the PLC effect at 77 K: the lower diffusion coefficient contributes to decreasing the DSA and inhibits the formation of solute clusters. The flow stress curve at 173 K is very similar to that at 298 K, except for the absence of the PLC effect. In addition, at 298 K, the solute atoms are able to diffuse through the matrix faster than the dislocations, which are then captured and temporarily pinned. Consequently, the stress increases, until it is reduced when the dislocations

Table 4 Estimated solid interdiffusion coefficients (D) for Mg and Si in Al matrix at different temperatures

Element	D in Al matrix/ ($m^2 \cdot s^{-1}$)	D/($m^2 \cdot s^{-1}$)		
		298 K	173 K	77 K
Mg	$6.23\times10^{-6}\exp(-13.83/T)$ [39]	5.94×10^{-6}	5.49×10^{-6}	4.58×10^{-6}
Si	$2.02\times10^{-4}\exp(-16.36/T)$ [40]	1.91×10^{-4}	1.74×10^{-4}	1.41×10^{-4}

are released from these diffusing solutes and/or clusters. This process occurs several times, resulting in the typical serrated effect of the PLC. According to RODRIGUEZ [22], there is a temperature range of occurrence of the PLC effect caused by DSA phenomenon. In general, at room temperature, due to the PLC effect, the work-hardening rate increases while Type-A and Type-E serrations are observed, which were found in AA6061 tensile tests.

4.3 Fracture and toughness at cryogenic temperatures

A homogeneous distribution of surface bands is observed in the neck region of the sample tested at 77 K. On the other hand, at 298 K the surface bands are more concentrated in the neck region, while the specimen tested at 173 K shows an intermediate behavior. Since the necking is late, high strain accumulation is allowed and a uniform distribution of surface bands in the specimen is observed [9]. Another crucial factor is the absence of DSA at 77 K, which facilitates the increase in the ductility.

The fracture surface morphology in Fig. 7 can be directly related with energy absorbed, even as the lateral roughness surface of the specimens is observed from the macroscopic and microscopic viewpoint. All these features are indicative of energy absorbed during the tests: at lower temperatures, the modulus of toughness is higher, and thus the size of dimples is changed, as presented in Fig. 8. This means that the AA6061 alloy could absorb more energy before failure at low temperatures. Another important finding can be observed in the trend at 298 K, in which the sample with the lower strain rate shows a slightly high modulus of toughness than the one with the higher strain rate. This behavior is very similar to that presented in Fig. 4 for the tensile behavior in terms of yield stress and ultimate tensile stress, and these characteristics are related to DSA phenomena. These findings presented here contribute in several ways to understand the effect of cryogenic temperatures on the mechanical and fracture behavior of the AA6061 alloy and provide a basis for mechanical processing at these temperatures.

5 Conclusions

(1) The mechanical properties of AA6061 alloy show a strong dependence on the temperature. The ultimate tensile stress is increased by 48% and 56% at 77 K, as compared to that at 298 and 173 K, respectively. Furthermore, the uniform elongation at 77 K reaches 0.35 of true plastic strain, whereas at 298 and 173 K it was close to 0.20. Partial suppression of dynamic recovery mechanisms, together with the inhibition of DSA contributes to these results. Thus, lower testing temperatures are related to an increase in the strain-hardening capacity, despite the slight increase in the flow stress.

(2) The strain rate sensitivity values are positive for the cryogenic tests (173 and 77 K) and negative for test at 298 K. In addition, the uniform elongation increases when the strain rate increases. The sample tested at a strain rate of 0.001 s^{-1} or less presents lower flow stress values, maintaining a high uniform elongation at 77 K.

(3) The mechanical behavior at the cryogenic temperatures is dominated by the dislocation glide and is succesfully described by the Johnson−Cook constitutive model:

$$\sigma=(530\varepsilon^{0.41})[1+0.02\ln(\dot{\varepsilon}/\dot{\varepsilon}_0)](1-T^{*0.7})$$

(4) For room temperature test, the correction of the strain rate factor C according to the empirical function $C=f(\dot{\varepsilon})$ is appropriate to describe the increase in flow stress due to DSA.

(5) The modulus of toughness at 77 K is higher than that at 173 and 298 K. Accordingly, at very low temperatures, the size of dimples in the fracture surface decreases, while their covered area increases. Moreover, the uniform elongation at 77 K is higher than that at 173 and 298 K, i.e., the AA6061 alloy is more ductile under the lower temperature.

Acknowledgments

We would like to acknowledge the São Paulo Research Foundation (FAPESP) (Grant No. 2014/15091-7 and 2016/10997-0) and the Conselho Nacional de Desenvolvimento Científico e Tecnológico - Brazil (CNPq) (Grant No. 449009/2014-9). This study was financed in part by the Coordenação de Aperfeiçoamento de Pessoal de Nível Superior - Brazil (CAPES) - Finance Code 001. Danielle Cristina Camilo MAGALHÃES acknowledges CNPq for her PhD scholarship (Grant No. 153181/2013-3).

References

[1] NAYAN N, MURTY S V S N, JHA A K, PANT B, SHARMA S C, GEORGE K M, SASTRY G V S. Mechanical properties of aluminium−copper−lithium alloy AA2195 at cryogenic temperatures [J]. Materials and Design, 2014, 58: 445−450.

[2] GLAZER J, VERZASCONI S L, DALDER E N C, YU W, EMIGH R A, RITCHIE R O, MORRIS J W Jr. Cryogenic mechanical properties of Al−Cu−Li−Zr alloy 2090 [C]//Advances in Cryogenic Engineering Materials. Springer US, 1986.

[3] HUAN X. Cryogenic tank and application of aluminium–lithium alloy [J]. Missiles Space Vehicles, 2001, 6: 008.

[4] PARK Doo-hwan, CHOI Sung-woong, KIM Jeong-hyeon, LEE Jae-myung. Cryogenic mechanical behavior of 5000- and 6000-series aluminum alloys: Issues on application to offshore plants [J]. Cryogenics, 2015, 68: 44−58.

[5] MANES A, PERONI L, SCAPIN M, GIGLIO M. Analysis of strain rate behavior of an Al 6061 T6 alloy [J]. Procedia Engineering, 2011, 10: 3477−3482.

[6] PICU R C, VINCZE G, OZTURK F, GRACIO J J, BARLAT F, MANIATTY A M. Strain rate sensitivity of the commercial aluminum alloy AA5182-O [J]. Materials Science and Engineering A, 2005, 390: 334−343.

[7] HADIANFARD M J, SMERD R, WINKLER S, WORSWICK M. Effects of strain rate on mechanical properties and failure mechanism of structural Al−Mg alloys [J]. Materials Science and Engineering A, 2008, 492: 283−292.

[8] CHEN Y, CLAUSEN A H, HOPPERSTAD O S, LANGSETH M. Stress−strain behavior of aluminum alloys at a wide range of strain rates [J]. International Journal of Solids and Structures, 2009, 46: 3825−3835.

[9] XU Z, ROVEN H J, JIA Z. Mechanical properties and surface characteristics of an AA6060 alloy strained in tension at cryogenic and room temperature [J]. Materials Science and Engineering A, 2015, 648: 350−358.

[10] HALIM H, WILKINSON D S, NIEWCZAS M. The Portevin−Le Chatelier (PLC) effect and shear band formation in AA5754 alloy [J]. Acta Materialia, 2007, 55: 4151−4160.

[11] PARK D, NIEWCZAS M. Plastic deformation of Al and AA5754 between 4.2 K and 295 K [J]. Materials Science and Engineering A, 2008, 491: 88−102.

[12] PARK D, NIEWCZAS M. Texture evolution in AA5754 alloy deformed in tension [J]. Materials Science and Engineering A, 2008, 497: 65−73.

[13] ESMAEILI S, CHENG L M, DESCHAMPS A, LLOYD D J, POOLE W J. The deformation behavior of AA6111 as a function of temperature and precipitation state [J]. Materials Science and Engineering A, 2001, 319−321: 461−465.

[14] STARKE E A Jr, STALEY J T. Application of modern aluminum alloys to aircraft [J]. Progress in Aerospace Sciences, 1996, 32(2−3): 131−172.

[15] ROVEN H J, NESBOE H, WERENSKIOLD J C, SEIBERT T. Mechanical properties of aluminum alloys processed by SPD: Comparison of different alloy systems and possible products areas [J]. Materials Science and Engineering A, 2005, 410−411: 426−429.

[16] PINK E, GRINBERG A. Practical aspects of the Portevin−Le Chatelier effect [J]. Aluminium, 1984, 60: 601−604.

[17] ZANG Wen-dan, BAI Pei-kang, YANG J, XU H, DANG Jin-zhi, DU Zhen-mi. Tensile behavior of 3104 aluminum alloy processed by homogenization and cryogenic treatment [J]. Transactions of Nonferrous Metals Society of China, 2014, 24(8): 2453−2458.

[18] PARK W S, CHUN M S, HAN M S, KIM M H, LEE J M. Comparative study on mechanical behavior of low temperature application materials for ships and offshore structures: Part I – Experimental investigations [J]. Materials Science and Engineering A, 2011, 528: 5790−5803.

[19] KUMAR M, SOTIROV N, GRABNER F, SCHNEIDER R, MOZDZEN G. Cryogenic forming behaviour of AW-6016-T4 sheet [J]. Transactions of Nonferrous Metals Society of China, 2017, 27(6): 1257−1263.

[20] ASTM E8/E8M−16ae1. Standard test methods for tension testing of metallic materials [S]. West Conshohocken, PA, ASTM International, 2016. https://www.astm.org/Standards/E8.htm

[21] ROBINSON M J, SHAW M P. Microstructural and mechanical influences on dynamic strain aging phenomena [J]. International Materials Reviews, 1994, 39(3): 113−122.

[22] RODRIGUEZ P. Serrated plastic flow [J]. Bulletin of Materials Science, 1984, 6(4): 653−663.

[23] ESTRIN Y, KUBIN L P. Plastic instabilities: Phenomenology and theory [J]. Materials Science and Engineering A, 1991, 137: 125−134.

[24] KOCKS U F, MECKING H. Physics and phenomenology of strain hardening: The FCC case [J]. Progress in Materials Science, 2003, 48(3):171−273.

[25] DOHERTY R D, HUGHES D A, HUMPHREYS F J, JONAS J J, JENSEN D J, KASSNER M E, KING W E, MCNELLY T R, MCQUEEN H J, ROLLET A D. Current issues in recrystallization: A review [J]. Materials Science and Engineering A, 1997, 238: 219−274.

[26] SAKAI T, BELYAKOV A, KAIBYSHEV R, MIURA H, JONAS J J. Dynamic and post-dynamic recrystallization under hot, cold and severe plastic deformation conditions [J]. Progress in Materials Science, 2014, 60: 130−207.

[27] MAGALHÃES D C C, KLIAUGA A M, FERRANTE M, SORDI V L. Plastic deformation of FCC alloys at cryogenic temperature: The effect of the stacking-fault energy on microstructure and tensile behavior [J]. Journal of Materials Science, 2017, 52: 7466−7478.

[28] CRIVOI M R, HOYOS J J, IZUMI M T, AGUIAR D J M, NAMUR R S, TERASAWA A L, CINTHO O M. In situ analysis of cryogenic strain of AISI 316L stainless steel using synchrotron radiation [J]. Cryogenics, 2020, 105: 103020.

[29] MAGALHÃES D C C, KLIAUGA A M, HUPALO M F, CINTHO O M, ROVERE C A D, FERRANTE M, SORDI V L. The influence of Cryo-ECAP and aging on the microstructure and mechanical behavior of the AA6061 Al alloy [J]. Materials Science and Engineering A, 2019, 768: 138485.

[30] IZUMI M T, QUINTERO J J H, CRIVOI M R, MAEDA M Y, NAMUR R S, AGUIAR D J M, CINTHO O M. In-situ X-ray diffraction analysis of face-centered cubic metals deformed at room and cryogenic temperatures [J]. Journal of Materials Engineering and Performance, 2019, 28(8): 4658−4666.
[31] van der BEUKEL A. Theory of the effect of dynamic strain aging on mechanical properties [J]. Physics of State Solid, 1975, 30: 197−206.
[32] KUBIN L P, CHIBAB K, ESTRIN Y. The rate dependence of Portevin−Le Chatelier Effect [J]. Acta Metallurgica, 1988, 36(10): 2707−2718.
[33] CONSIDÈRE A. Memoir on the use of iron and steel in construction [J]. Ann Ponts et Chaussées, 1885, 9: 574−775.
[34] JOHNSON G R, COOKS W H. Fracture characteristics of three metals subjected to various strains, strain rates, temperatures and pressures [J]. Engineering Fracture Mechanics, 1985, 21(1): 31−48.
[35] YE T, LI L, GUO P, XIAO G, CHEN Z. Effect of aging treatment on the microstructure and flow behavior of 6063 aluminum alloy compressed over a wide range of strain rate [J]. International Journal of Impact Engineering, 2016, 90: 72−80.
[36] SANCHO R, CENDÓN D, GÁLVEZ F. Flow and failure of an aluminum alloy from low to high temperature and strain rate [C]//Lugano, Switzerland: EPJ Web Conference, 2015: 04055.
[37] VOYIADJIS G Z, SONG Y, RUSINEK A. Constitutive model for metals with dynamic strain aging [J]. Mechanics of Materials, 2019, 129: 352−360.
[38] LI Z X, ZHAN M, FAN X G, TAN J Q. A modified Johnson−Cook model of as-quenched AA2219 considering negative to positive strain rate sensitivities over a wide temperature range [J]. Procedia Engineering, 2017, 207: 155−160.
[39] XIE F, YAN X, DIING L, ZHANG F, CHEN S, CHU M G, CHANG Y A. A study of microstructure and microsegregation of aluminum 7050 alloy [J]. Materials Science and Engineering A, 2003, 355: 144−153.
[40] FUJIKAWA S I, HIRANO K I, FUKUSHIMA Y. Diffusion of silicon in aluminum [J]. Metallurgical Transactions A, 1978, 9: 1811−1815.

Al−Mg−Si 合金在低温下的流变行为和断裂

Danielle Cristina Camilo MAGALHÃES, Andrea Madeira KLIAUGA, Vitor Luiz SORDI

Department of Materials Engineering, Federal University of São Carlos−UFSCar,
Rod. Washington Luiz, km 235, 13565-905, São Carlos–SP, Brazil

摘　要：研究 AA6061 合金的拉伸和断裂行为，为该合金在低温范围内的拉伸和断裂行为提供定量数据。在 298 K、173 K 和 77 K 下对铝合金进行固溶处理，然后在应变速率为 0.1~0.0001 s^{-1} 条件下进行拉伸试验。结果表明，77 K 时 Portevin−Le Chatelier (PLC) 效应和动态应变时效(DSA)被抑制。相反，298 K 时，观察到 PLC 效应的特征，即明显的锯齿状流变。77 K 固溶处理后样品的拉伸性能与 173 K 和 298 K 处理的样品拉伸性能相比，强度、伸长率、韧性模量、应变硬化指数和应变速率敏感性同时提高，这与低温下动态回复速率的降低有关。与之相对应，断口形貌结果显示，77 K 处理的样品韧窝尺寸减小，而韧窝覆盖的面积增加。173 K 和 77 K 处理的样品中 DSA 被抑制，其实验结果与 Johnson−Cook 模型模拟结果吻合较好。

关键词：低温；铝合金；流变行为；应变速率敏感性；加工硬化行为；Johnson−Cook 模型；断裂

(Edited by Bing YANG)